Research Article

Xiaodong Chen#, Zhong-Tao Yang#, Nannan Wang#, Xin Gao#, Gang Wang, Chunyu Song*, Yunfeng Liu, and Lifeng Cui*

Fabrication of Ag/ZnO hollow nanospheres and cubic TiO_2/ZnO heterojunction photocatalysts for RhB degradation

https://doi.org/10.1515/ntrev-2021-0089
received August 27, 2021; accepted September 10, 2021

Abstract: ZnO nanomaterials with the stereochemical structure were becoming a research focus in the scope of photocatalytic materials, but the ZnO was sensitive to UV light rather than the solar light source, which considerably prohibited its extended application. ZnO nanomaterials coupled with other nanomaterials could generate the alternative composite heterojunction nanomaterials to promote the photocatalytic activity. Herein, we reported two facile and feasible synthesis methods to fabricate TiO_2/ZnO cube nanocomposites and Ag/ZnO hollow spheres by hydrothermal reaction and chemical deposition, respectively. In this regard, these composited nanomaterials have been successfully fabricated with high purities, good morphology, and crystal structure. Noticeably, in contrast with TiO_2/ZnO and Ag/ZnO bulk nanocomposites, the Ag/ZnO hollow spheres could offer the higher activity for RhB degradation under the visible light. Moreover, the photocatalytic performance of Ag/ZnO for RhB degradation could be improved synergistically, and the effect of RhB degradation was highest when the Ag mass ratio was modulated at 10% in the sample. Furthermore, it remained a high photocatalytic efficiency even after four cycles. This protocol provided an approvable approach to fabricate efficient photocatalysts with persistent photostability in the wastewater treatment process.

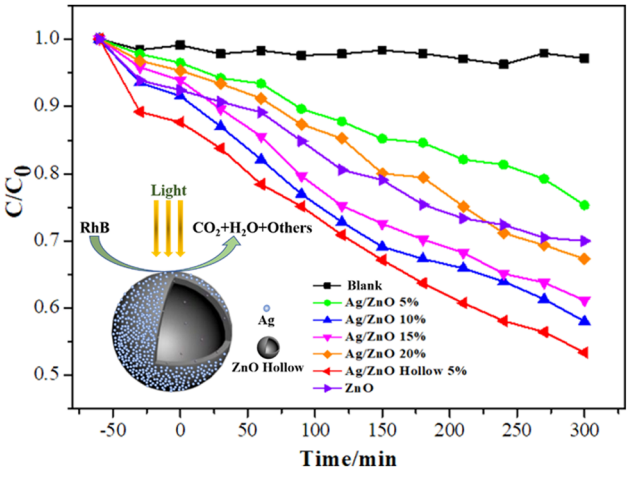

Graphical abstract

Keywords: Ag/ZnO, TiO_2/ZnO, hollow spheres, nanocomposites, photocatalysis, RhB degradation

1 Introduction

Photocatalysis was typically considered as the prominent technologies for the application in the scope of environmental pollutants elimination, hydrolysis, CO_2 reduction, metal corrosion, and protection [1–4]. Their practical value and application potential have triggered continuous interests in developing effective and stable photocatalysts for pollutants reduction [5]. For decades, semiconducting metal oxides have widely developed for

# These authors contributed equally to this work.

* **Corresponding author: Chunyu Song,** Southern Marine Science and Engineering Guangdong Laboratory (Zhanjiang), Zhanjiang 524000, China, e-mail: 1196198142@qq.com
* **Corresponding author: Lifeng Cui,** School of Materials Science and Engineering, Dongguan University of Technology, Dongguan 523808, China, e-mail: lcui@dgut.edu.cn
Xiaodong Chen, Xin Gao: Southern Marine Science and Engineering Guangdong Laboratory (Zhanjiang), Zhanjiang 524000, China
Zhong-Tao Yang: Marine Biomedical Research Institute of Guangdong Zhanjiang, Zhanjiang 524023, China
Nannan Wang: College of Chemistry and Material Engineering, Chao Hu University, Hefei 238000, China
Gang Wang: College of Chemistry and Chemical Engineering, Henan University of Technology, Zhengzhou 450001, China
Yunfeng Liu: Research Institute of Natural Gas Technology, Southwest Oil and Gas Field Company of PetroChina, Chengdu 610213, China

their favorable properties of suitable redox potentials, high photosensitivity, and low expenditure [6]. Especially for ZnO, it often exhibited the desirable photocatalytic activity due to its suitable band-gap energy and superior physicochemical properties [7–10]. However, the low separating efficiency of photogenerated charges and poor quantum utilization rate disapproved its further application to a certain extent [11–13].

Various strategies have been attempted to address the aforementioned challenges, including doping, constructing composite inhibition, and designing novel nanostructures [14–16]. Among them, constructing composite heterojunction between ZnO and TiO_2 has been demonstrated to be a facile and effective strategy for increasing the photocatalytic performance [5,17]. Besides, the closeness of energy band and forbidden bandwidth between ZnO and TiO_2 could make them well engage to form a composite material, which could become a promising candidate for RhB degradation [19–21]. Nevertheless, the dilemma of insufficient controllable preparation method restricted its further photocatalytic application due to the physical incompatibility during the preparation process [18–21]. Therefore, the architecture development of heterojunction nanomaterials as photocatalysis was highly desirable to improve photocatalytic efficiency.

Benefiting from the higher surface areas, controllable pore sizes, good dispersion, and high sensitivity, the hollow ZnO could also be utilized to favor the decomposition of pollutants in the solvent during the photocatalytic process [6,22–26]. Besides the introduction of TiO_2 into ZnO, the composite metals into the ZnO including Ag, Pd, Pt, and Au have been extensively reported so far [27]. Comparatively, Ag has many advantages, such as low expenditure, less toxic, and easy to industrialize, which could be used to improve the activity of photocatalyst *via* hybridation [28–30]. Herein, we disclosed new strategies for photocatalytic RhB degradation by virtue of TiO_2/ZnO and Ag/ZnO nanocomposites, which were synthesized through two effective methods of hydrothermal reaction and chemical deposition, respectively. Scanning electron microscopy (SEM), X-ray diffraction (XRD), and UV-vis optical absorption confirmed these nanocomposites with good morphology, crystal structure, and high purities. Photocatalytic degradation of RhB was studied in the irradiation with visible light. What's more, the photocatalytic efficiency and photostability for Ag/ZnO with different mass ratios were also investigated.

2 Experimental

2.1 Materials

The reagents such as $CaCl_2$, PEG-1000, $Ti(OC_4H_9)_4$, $CaTiO_3$, KOH, and PVP were of analytical grade, obtained from Aladdin Company and used without further purification.

2.2 Chemical synthesis

2.2.1 Synthesis of TiO_2

A mixture of 0.11 g $CaCl_2$, 0.5 g PEG-1000, and 0.33 mL Ti $(OC_4H_9)_4$ was dissolved in 35 mL absolute ethanol and stirred at 25°C for 20 min. A total of 0.24 g NaOH was added under stirring. Then, the mixture was transferred to a 50 mL autoclave and held at 180°C for 15 h in an electric oven. After natural cooling to room temperature, the samples were washed with ethanol, deionized water, and then centrifuged and recovered to obtain the $CaTiO_3$ sample. Subsequently, 0.075 g $CaTiO_3$ and 0.34 g of Na_2EDTA were dissolved in 40 mL of ionized water and ethylene glycol for ultrasonic treatment. Then, the solution was poured into a 50 mL autoclave and meantime raised the temperature to 180°C in a closed environment for 12 h. When cooled down, the sample was washed thoroughly with deionized water and ethanol and then dried the material by controlling the oven temperature at 80°C for 12 h, which was subsequently annealed at 400°C for 2 h. Eventually, the TiO_2 sample was successfully prepared.

2.2.2 Synthesis of ZnO seed crystal

A total of 0.115 g zinc acetate was added into 125 mL absolute ethyl alcohol, and then, the solution was stirred evenly at 60°C until the zinc acetate was completely dissolved. A total of 0.055 g KOH was dissolved into 65 mL of absolute ethyl alcohol, and the, it was stirred evenly until the KOH was completely dissolved, then the solution of KOH was transferred into the solution of zinc acetate at 60°C with stirring, and the sol–gel solution was finally obtained by stirring for 2 h at 60°C, and the seed solution of ZnO was used for the next step.

2.2.3 Synthesis of TiO_2/ZnO

The fabricated TiO_2 was weighed and added into 5 g/L PVP aqueous solution and stirred for 4 h in a shaker. After the TiO_2 was fully coated by PVP, the solution was centrifuged and dried. The dried intermediate sample was dispersed in 20 mL of ZnO seed solution and placed in a shaker at room temperature for 4 h. Then, the intermediate sample was obtained by centrifugal washing and dried. This sample was added into 20 mL of a 10 mM $Zn(NO_3)_2{\cdot}6H_2O$ growth medium and HMT growth medium, incubated at 85°C for 8 h, and then washed with deionized water and anhydrous ethanol. Finally, TiO_2/ZnO photocatalyst was obtained by drying at 80°C for 4 h.

2.2.4 Synthesis of C ball

A mixture of 4 g anhydrous glucose and 150 mL deionized water was stirred, placed in a polytetrafluoroethylene reaction kettle, and stirred at 180°C for 10 h. The sample was centrifuged and washed by using deionize water and ethanol and then dried in an oven at 60°C. Finally, the C ball was successfully made for standby.

2.2.5 Synthesis of hollow ZnO

A mixture of 0.1 g C ball, 0.298 g $Zn(NO_3)_2.6H_2O$, and 7 g hexamethylenetetramine (HMT) was added into 100 mL ethanol. After ultrasonic treatment for 30 min, the mixture was put into the water bath and stirred for 2 h at 60°C, centrifuged three times with ethanol, and dried. The dried material was put into a muffle furnace, which had a temperature program of raising to 550°C at a speed of 5°C/min and maintained for 2 h to get hollow ZnO. Then, it was kept in the air for 2 h to remove the organic template and promote the ZnO film crystallization, leaving only a closed ZnO hollow spheres array.

2.2.6 Synthesis of hollow Ag/ZnO

A total of 0.1 g hollow ZnO was dispersed into 50 mL of deionized water containing 0.0075–0.030 g $AgNO_3$, respectively, followed by the addition of 10 mL methanol under continuous stirring. Then, the solution was put into a xenon lamp (an instrument for photocatalytic degradation of RhB) and irradiated it for 30 min with revolution and rotation, followed by centrifugally washing for three times using water and ethanol. After the samples were dried, the hollow ZnO with 5–20% Ag deposited was obtained. The hollow Ag/ZnO nanocomposites were fabricated through the aforementioned three processes, as illustrated in Figure 1.

2.2.7 Synthesis of ZnO bulk

A mixture of 0.298 g $Zn(NO_3)_2.6H_2O$ and 7 g HMT was put into 100 mL ethanol. After ultrasonic treatment for 30 min, this solution was added into the water bath, stirred for 2 h at 60°C, centrifuged for three times with ethanol and dried, then placed in a muffle furnace to raise 550°C at a speed of 5°C/min, and maintained for 2 h to synthesize ZnO bulk.

2.3 Characterization

The surface and interior morphology were checked by using a field-emission scanning electron microscope (FESEM) (TESCAN VEGA3) and a transmission electron microscope (TEM) (JEM-2100). The crystallinity and phase composition of all products were characterized by X-ray diffraction (Bruke-D8 ADVANCE) with a Cu-Kα source of radiation (λ = 1.5418 Å). The average crystallite size of the Ag nanoparticles was determined using the Scherrer formula (1):

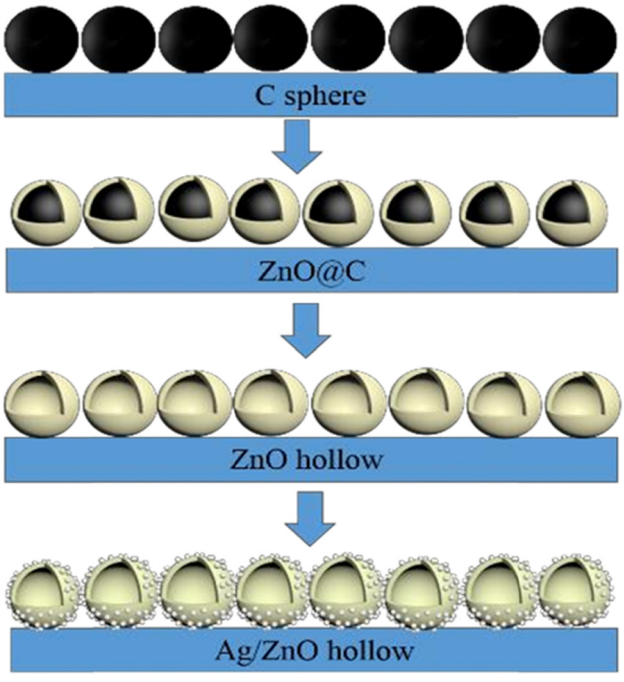

Figure 1: The synthesis process of hollow Ag/ZnO nanocomposite.

$$R = \frac{K\lambda}{\beta c \cos\theta}, \quad (1)$$

where K was the value of the Scherrer constant, λ was the wavelength of the X-ray, and c is the full width of the half peak (111) with radius (1/2).

The optical properties were characterized by a UV-vis diffuse reflectance spectrophotometer (Varian Cary 500) with the samples supported on ZnO. Nitrogen adsorption–desorption isotherms were measured at 77 K on a Micromeritics Tristar 3000 instrument. The thermal spectrometer using a laser with an excitation wavelength of 532 nm was used to record Raman spectra.

2.4 Photocatalytic activity

The photocatalytic degradation of organic pollutant rhodamine B was studied. The hollow Ag/ZnO with different mass ratios of Ag was prepared, and the hollow Ag/ZnO spheres with the best morphology and mass ratio were characterized and analyzed. The photocatalytic experiments were carried out in the JH-GHXII catalytic reactor. The photocatalytic degradation of organic pollutants RhB was used to measure the photocatalytic performance of the material, and the TiO_2/ZnO hollow spheres were also characterized and analyzed. Specifically, 30 mg TiO_2/ZnO was dispersed into 5 mg/L RhB aqueous solution. Before irradiation, the dark reaction was carried out for 1 h to make the solution reach adsorption–desorption equilibrium. Then, a 500 W xenon lamp was turned on, a filter with a wavelength of 420 nm was put on, and the material was kept stirring for photocatalytic reaction. A total of 0.3 mL solution was taken out from the reactor every 1 minute. After the sample was centrifuged, the separated liquid-phase products were taken for the absorbance experiment. The degradation rate of the photocatalytic material was calculated *via* the following equation:

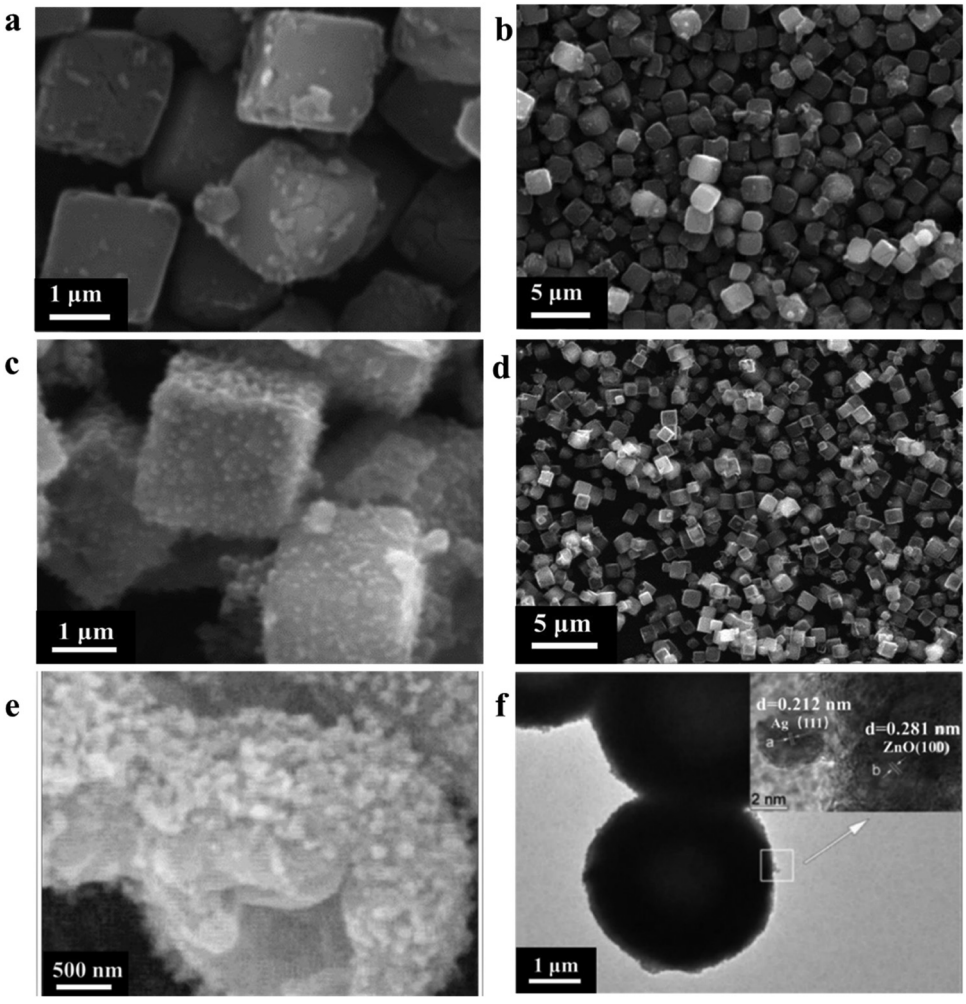

Figure 2: SEM images of pure TiO_2 cubic (a and b) and TiO_2/ZnO (c and d); SEM (e) and TEM images of 10% Ag/ZnO hollow spheres (f).

$$R = (A - A_0)/A, \quad (2)$$

where R was the degradation rate; A_0 and A represented the absorbance of rhodamine B solution before and after degradation, respectively.

After the photocatalytic degradation experiments were finished, the catalyst in the RhB aqueous solution was centrifuged by absolute ethyl alcohol and deionized water, dried, and then dried in an oven at 60°C to test the repeatability and stability. Finally, this material was found still served as the photocatalyst in the later period.

3 Results and discussion

The SEM photograph of TiO_2 surface morphology is shown in Figure 2(a) and (b). It can be clearly found that the as-fabricated TiO_2 was cubic, and some broken samples were seen in the nanocubic TiO_2 particles, some samples had cracks on the surface, and the overall size of each cube was 1–3 μm^3. Figure 2(c) and (d) show a SEM image of the TiO_2/ZnO nanocomposite. It was demonstrated that the surface of the TiO_2/ZnO sample was rough, and ZnO nanoparticles were densely grown and uniformly distributed on the surface of the cube TiO_2. Interestingly, although the TiO_2/ZnO nanocubes were closely stacked together, their shape still presented a more regular cubic structure. Furthermore, SEM images of the morphology of Ag/ZnO photocatalyst are shown in Figure 2(e). It can be detected that the ZnO delivered the evident hollow spheres shape and the size of the sphere was 1–2 μm. In addition, numerous Ag nanoparticles were highly dispersed on the surface of ZnO hollow spheres, and the sizes of the spheres ranged from 5 to 10 nm. The representative TEM and high-resolution TEM (HR-TEM) images of Ag/ZnO are displayed in Figure 2(f). The low-magnification TEM image clearly demonstrates that the Ag/ZnO was identified as the hollow spheres, where its surface consisted of a layer of ZnO particles. Furthermore, the HRTEM image disclosed that the Ag was attached on the hollow sphere surface, as evidenced by the lattice fringes of Ag (111) at 0.212 nm and ZnO (100) at 0.281 nm [5,31–33].

The powder XRD patterns of TiO_2 and TiO_2/ZnO nano-heterojunction photocatalysts were displayed in Figure 3. More specifically, the TiO_2 precursor had several characteristic peaks at 2θ = 27.4°, 36.1°, 41.4°, 54.3°, and 69.3°, which were assigned to the (101), (004), (200), (211), and (204) plane of rutile TiO_2, respectively. From the XRD patterns of ZnO/TiO_2 nano-heterojunction composites, some of the appeared peaks belonged to the rutile TiO_2, and the additional peaks at 2θ = 31.8°, 34.5°, 47.6°, 56.7°,

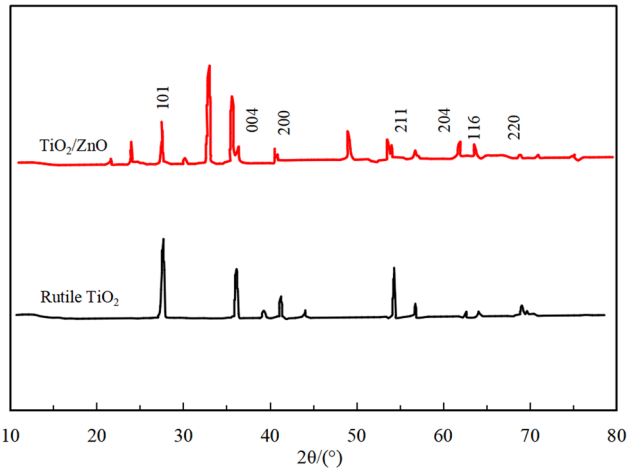

Figure 3: XRD pattern of TiO_2 and TiO_2/ZnO.

and 62.9° were attributed to (100), (002), (102), (110), and (103) planes of ZnO, respectively, with cubic phase (PDF card 36-1451), which denoted that the nano-TiO_2/ZnO photocatalyst was successfully fabricated [34]. From the comparison of Figure 4(a) and (b), the XRD pattern of ZnO bulk was similar to that of ZnO hollow spheres, and the five diffraction peaks at 31.71°, 34.32°, 36.22°, 47.43°, and 56.65° can be ascribed to the (100), (002), (101), (102), and (110) planes of ZnO with cubic phase, respectively. The main crystallographic planes were (101) plane, thus demonstrating the preferential growth of ZnO on the (101) crystal plane. In comparison, the sharper diffraction peaks of ZnO hollow spheres signified a better crystallinity. The XRD patterns of ZnO modified with Ag are shown in Figure 4(c) and (d). It was depicted that the new diffraction peaks of appeared at 38.6°, 44.9°, 64.8°, and 77.6° were indexed to the (111), (200), (220), and (311) planes of Ag (PDF No. 04-783). Moreover, after the deposition of Ag, the position of ZnO diffraction peaks did not change, suggesting that Ag did not enter the crystal lattice of ZnO, but adhered to the ZnO surface. Besides, the peak intensity was decreased due to the encapsulation of Ag on the outer surface of ZnO. Since the coated Ag particles were nanosized, the peaks of the composite particles become broadened. Accordingly, the Ag/ZnO composite was well formed.

There was a close relationship between the bandgap and the photocatalytic properties of semiconductor photocatalysts. When the photoresponse range of the materials in the visible light region shifted toward the long wavelength direction, the photocatalytic properties would certainly be better. Figure 5 shows the UV-vis diffuse reflectance spectra of ZnO bulk, ZnO hollow spheres, 10% Ag/ZnO bulk, and 10% Ag/ZnO hollow spheres.

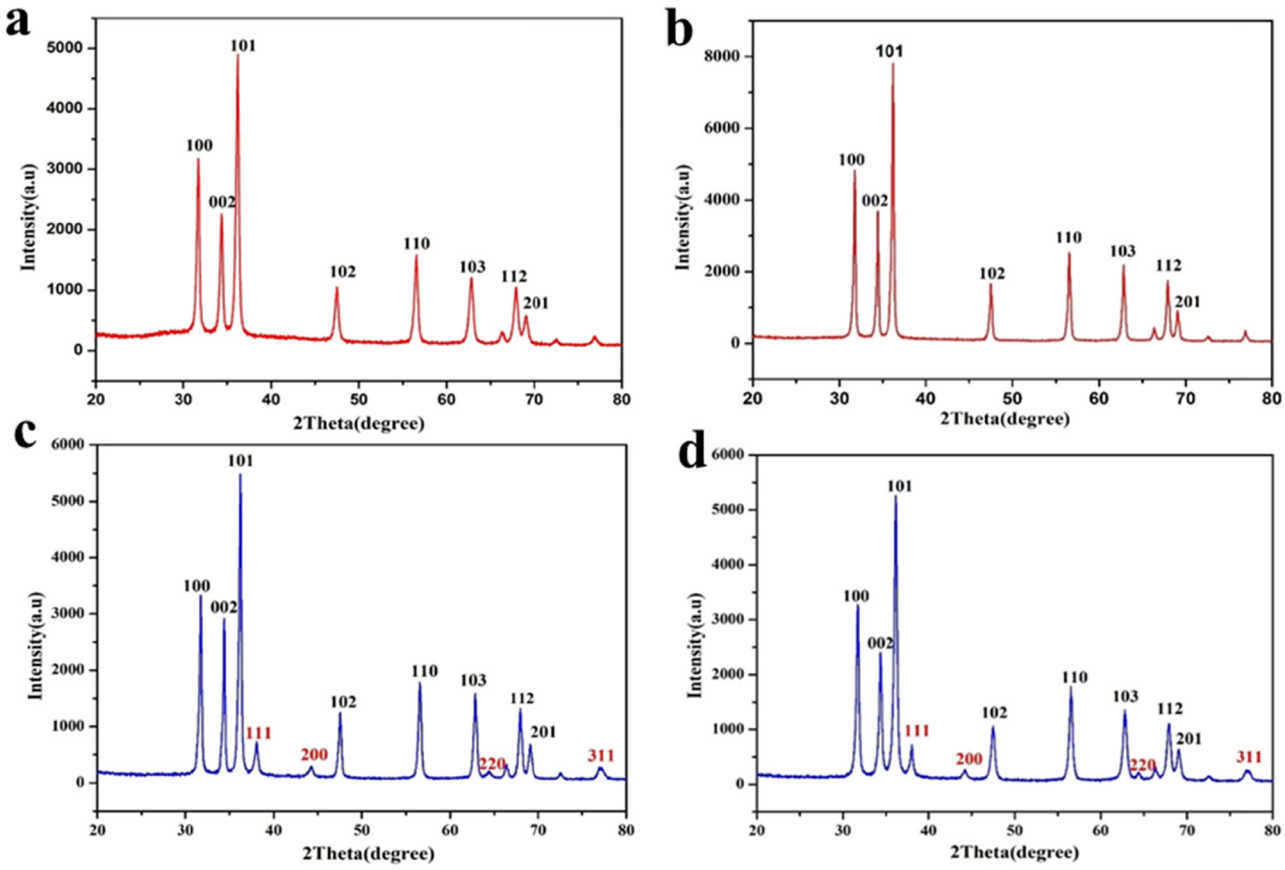

Figure 4: XRD pattern of ZnO bulk (a), ZnO hollow sphere (b), 10% Ag/ZnO bulk (c), and 10% Ag/ZnO hollow sphere (d).

The characteristic absorption peak of pure ZnO bulk appeared at 380 nm, which was consistent with its intrinsic absorption band at 390 nm. The composite nanomaterial of Ag/ZnO hollow spheres presented the adsorption peak shift from 380 to 428 nm after the Ag particles deposited on the ZnO surface, which was attributed to the strong interaction between them [35,36]. Compared with Ag/ZnO hollow spheres, the absorption peak of Ag/ZnO bulk had blue-shift to a certain degree due to the weaker interaction existing between them. These results demonstrated that Ag/ZnO hollow spheres could exhibit favorable photocatalytic properties because of its adsorption peak at the long wavelength range.

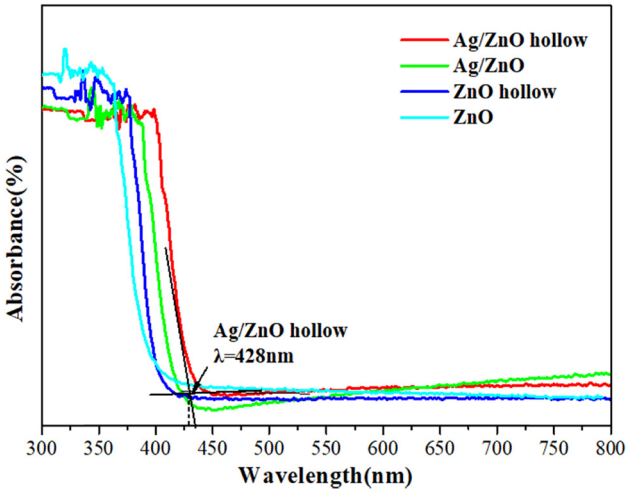

Figure 5: UV-Vis diffuse reflectance spectra of pure ZnO bulk, ZnO hollow spheres, 10% Ag/ZnO bulk, and 10% Ag/ZnO hollow spheres.

The nitrogen adsorption–desorption isotherms of ZnO bulk, ZnO hollow spheres, 10% Ag/ZnO bulk, and 10% Ag/ZnO hollow spheres are shown in Figure 6(a), which were used to determine the specific surface area by the BET method. All the samples exhibited a typical IV-type isotherm with the H_3 hysteresis loop, confirming the existence of both mesopores and macropores in these samples. The pore size distribution curves of these samples illustrated in Figure 6(b) presented the pores size distribution from 5 to 130 nm. Correspondingly, the BET surface of ZnO bulk, ZnO hollow spheres, 10% Ag/ZnO bulk, and 10% Ag/ZnO hollow spheres had been calculated to be 8.7, 13.7, 11.2, and 4.5 m^2/g, respectively. This result disclosed

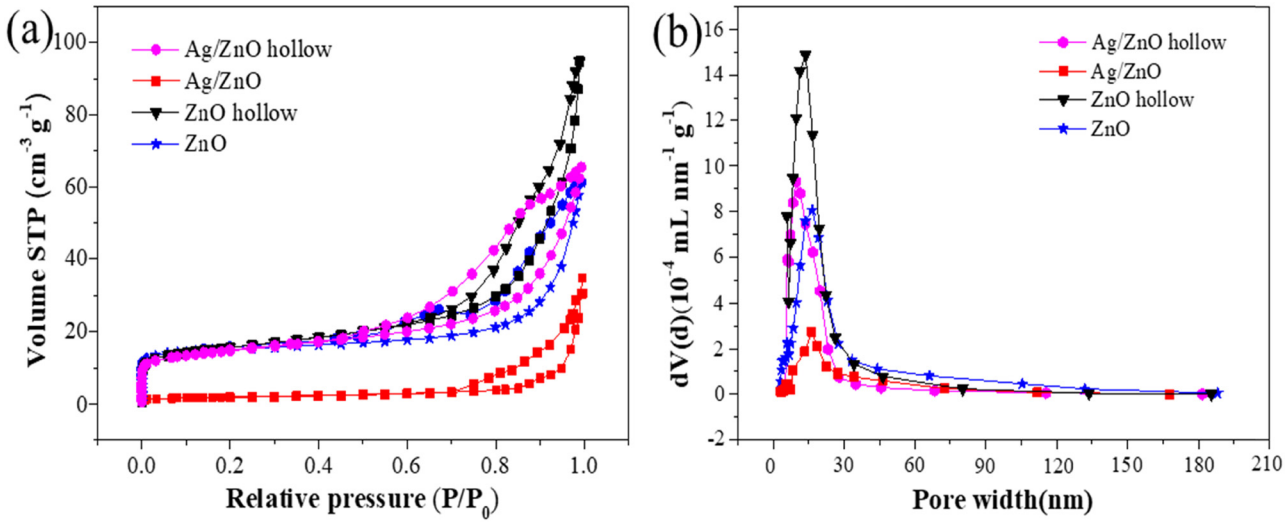

Figure 6: (a) N_2 adsorption–desorption isotherms and (b) corresponding pore volume *vs* pore size distribution of ZnO bulk, ZnO hollow spheres, 10% Ag/ZnO bulk, and 10% Ag/ZnO hollow spheres.

that 10% Ag/ZnO hollow spheres possessed the larger surface area among the aforementioned samples due to their abundant pores surviving on the hollow structure surface, which was beneficial to the increase of the photocatalytic activity.

The degradation efficiency of pollutant RhB on ZnO, TiO_2, TiO_2/ZnO catalyst under visible light irradiation is shown in Figure 7(a). In the blank experiment, the concentration of RhB had no obvious fluctuation in four curves, illustrating that the self-decomposition of RhB pollutants under visible light could be ignored. However, when ZnO catalyst was added, the RhB was degraded slowly and the relevant degradation rate was only about 5% after 120 min. Meantime, the RhB degradation rate of TiO_2 was about 17%, and the result was also not desirable. Moreover, the RhB degradation rate of TiO_2/ZnO had no significant change, which was even lower than that of pure TiO_2 in the same period after repeating results of many experiments. Hence, we supposed that ZnO formed a film on the surface of TiO_2, which made TiO_2 unable to make full use of visible light for photocatalytic activities and thus reduced photocatalytic performance. Therefore, excluding the error of data, it could be judged that the photocatalytic effect of TiO_2/ZnO cubic nano-heterojunction composite material was not as expected. Significantly, it should be noted that the RhB degradation rates of Ag/ZnO photocatalysts are shown in Figure 7(b) and (c). The photocatalytic efficiency of Ag/ZnO hollow spheres photocatalysts is higher than that of Ag/ZnO bulk photocatalysts, which were also better than both ZnO and blank experiment. Because when Ag was loaded, the electrons of ZnO were excited under visible light and then jumped to its conduction band, and simultaneously, the Ag could temporarily store photogenerated electrons and improve its photocatalytic performance. More specifically, the overall trend of the curves was that the degradation rate of pollutant RhB changed significantly in the first 5 min, and then, the degradation rate began to slow down, mainly because at the beginning of the experiment, the amounts of pollutants were large, so the opportunity and area of contact with catalyst were large, which led to faster degradation in the early stage. When the reaction went to the later stage, the concentration of RhB pollutants was low, and the number of molecules that could react was reduced, so the degradation efficiency would become worse. Moreover, the photocatalytic performance of Ag/ZnO hollow spheres was the best when the loading mass fraction of Ag was 10%. As the mass fraction of Ag increased from 0 to 10%, the photocatalytic effect increased all the time. What's more, as the doping amount of Ag increased from 10% to 20%, the photocatalytic activities decreased gradually. Accordingly, the loading amount of Ag over the ZnO determined the photocatalytic activity of RhB degradation. This was because that the doping of Ag over the ZnO was conductive to promote its separation of photocarriers, which could prolong its lifetime and transmission time, thus enhancing its photocatalytic activities of RhB degradation. Moreover, the stability of the photocatalyst was the basic requirement for its practical application in the future. For the 10% Ag/ZnO hollow sphere photocatalyst, we tested repeatedly and found that its RhB degradation

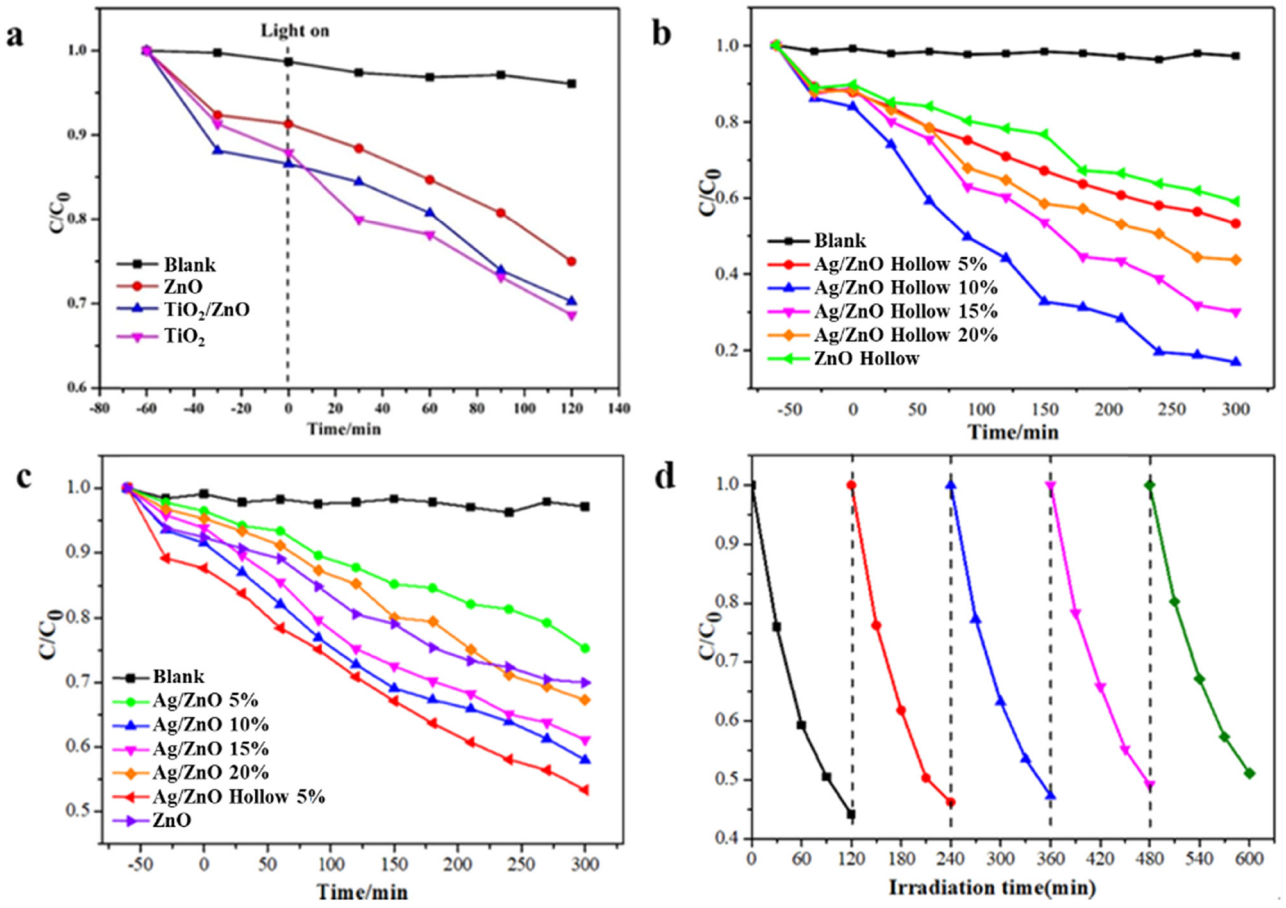

Figure 7: Degradation rate of RhB by ZnO, TiO_2, and TiO_2/ZnO (a); pure ZnO hollow spheres and Ag/ZnO hollow spheres with different mass ratios (b); pure ZnO bulk and Ag/ZnO with different mass ratios under visible light (c); and cyclic photocatalytic performance diagram of 10% Ag/ZnO hollow sphere photocatalyst (d).

rate was basically not reduced even after five cycles, which remained at a high level of 90%, displaying its good photostability (Figure 7d).

4 Conclusion

In summary, we have demonstrated the synthesis of TiO_2/ZnO and hollow Ag/ZnO for RhB degradation through two facial methods of low-temperature hydrothermal and chemical deposition, respectively. Scanning electron microscopy (SEM), X-ray diffraction (XRD), and UV-Vis optical absorption confirmed that these composited nano-materials have good morphology, crystal structure, and high purities. The modified photocatalysts for RhB degradation were researched under visible light, which revealed that the TiO_2/ZnO has almost the same photocatalytic activities for RhB degradation. However, the Ag/ZnO hollow spheres could synergistically enhance the photocatalytic performance. An optimal concentration of 10% Ag loaded on the hollow-sphere heterojunction material shows the highest photocatalytic efficiency. Noticeably, its photocatalytic activity still remains excellent even after four cycles. More importantly, this methodology represented an effective solution to obtain good photostability of Ag/ZnO hollow spheres, enriching the arsenal of ZnO heterojunction nanomaterials, which also showed great potential for its application in wastewater treatment.

Funding information: This project is financially supported by the Startup Research Fund of Dongguan University of Technology (KCYKYQD2019015), the Postdoctoral Startup Research Fund of Dongguan University of Technology (196100040019), the Guangdong Basic and Applied Basic Research Foundation (No. 2020A1515110221), the National Natural Science Foundation of China (No.U1904171), the Science and Technology Foundation of Henan Province (Nos. 182102410092), and the Young Backbone Teachers Training Program Foundation of Henan University of Technology.

Author contributions: X.C.: conceptualization; C.S. and Z.Y.: methodology; N.W.: validation; X.C. and X.G.: formal analysis; X.C., N.W., and Z.Y.: investigation; N.W. and L.C.: resources; Y.L.: data curation; X.C. and X.G.: writing–original draft preparation; N.W., and X.G.: writing–review and editing; N.W. and L.C.: supervision; C.S.: project administration; X.C., N.W., Y.L., and L.C.: funding acquisition. All authors have accepted responsibility for the entire content of this manuscript and approved its submission.

Conflict of interest: The authors declare no conflict of interest.

References

[1] Gnayem H, Uvarov V, Lahad O, Sasson Y. Hybrid bismuth oxyhalides@gypsum as self-cleaning composites: novel aspects of a sustainable photocatalytic technology for solar environmental cleanup. RSC Adv. 2015;5(82):66650–6.

[2] Liu YX, Sun ZX, Hu YH. Bimetallic cocatalysts for photocatalytic hydrogen production from water. Chem Eng J. 2021;409:128250.

[3] Dou YB, Zhou AW, Yao YC, Lim SY, Li JR, Zhang WJ. Suppressing hydrogen evolution for high selective CO_2 reduction through surface-reconstructed heterojunction photocatalyst. Appl Catal B: Env. 2021;286:119876.

[4] Tahir MB, Asiri AM, Malik MF, Khalid NR, Iqbal T, Rafique M, et al. Role of nano-photocatalysts in detoxification of toxic heavy metals. Curr Anal Chem. 2021;17:126–37.

[5] Li M, Zhang SB, Li LW, Han JY, Zhu XL, Ge QF, et al. Construction of highly active and selective polydopamine modified hollow ZnO/Co_3O_4 p-n heterojunction catalyst for photocatalytic CO_2 reduction. ACS Sustain Chem Eng. 2020;8:11465–76.

[6] Septiani NLW, Saputro AG, Kaneti YV, Maulana AL, Fathurrahman F, Lim H, et al. Hollow zinc oxide microsphere-multiwalled carbon nanotube composites for selective detection of sulfur dioxide. ACS Appl Nano Mater. 2020;3:8982–96.

[7] Sun YY, Zhu L, Lu HJ, Wang RW, Lin S, Jiang DZ, et al. Sulfated zirconia supported in mesoporous materials. Appl Catal a-Gen. 2002;237:21–31.

[8] Wang YQ, Zhang RR, Li JB, Li LL, Lin SW. First-principles study on transition metal-doped anatase TiO_2. Nanoscale Res Lett. 2014;9:46.

[9] Linsebigler AL, Lu GQ, Yates JT. Photocatalysis on TiO_2 surfaces – principles, mechanisms, and selected results. Chem Rev. 1995;95:735–58.

[10] Bickley RI, Jayanty RKM, Navio JA, Real C, Macias M. Photooxidative fixation of molecular nitrogen on TiO_2 (Rutile) surfaces – the nature of the adsorbed nitrogen-containing species. Surf Sci. 1991;251:1052–6.

[11] Deng HZ, Xu FY, Cheng B, Yu JG, Ho WK. Photocatalytic CO_2 reduction of C/ZnO nanofibers enhanced by an Ni-NiS cocatalyst. Nanoscale. 2020;12:7206–13.

[12] Zhao H, Dong YM, Jiang PP, Wang GL, Miao HY, Wu RX, et al. Light-assisted preparation of a ZnO/CdS nanocomposite for enhanced photocatalytic H-2 evolution: an insight into importance of *in situ* generated ZnS. ACS Sustain Chem Eng. 2015;3:969–77.

[13] Bockmeyer M, Lobmann P. Crack formation in TiO_2 films prepared by sol–gel processing: Quantification and characterization. Thin Solid Films. 2007;515:5212–9.

[14] Yu WL, Xu DF, Peng TY. Enhanced photocatalytic activity of g-C_3N_4 for selective CO_2 reduction to CH_3OH *via* facile coupling of ZnO: a direct Z-scheme mechanism. J Mater Chem A. 2015;3:19936–47.

[15] Li P, Zhou Y, Li HJ, Xu QF, Meng XG, Wang XY, et al. All-solid-state Z-scheme system arrays of $Fe_2V_4O_{13}$/RGO/CdS for visible light-driving photocatalytic CO_2 reduction into renewable hydrocarbon fuel. Chem Commun. 2015;51:800–3.

[16] Wang C, Xu BQ, Wang XM, Zhao JC. Preparation and photocatalytic activity of ZnO/TiO_2/SnO_2 mixture. J Solid State Chem. 2005;178:3500–6.

[17] Mondal S, Mitra P. Preparation of cadmium-doped ZnO thin films by SILAR and their characterization. B Mater Sci. 2012;35:751–7.

[18] Han JH, Liu ZF. Optimization and modulation strategies of zinc oxide-based photoanodes for highly efficient photoelectrochemical water splitting. ACS Appl Energ Mater. 2021;4:1004–13.

[19] Zhang JX, Luo KY, Zhao K, Hu WY, Yuan H, Liu YT, et al. A synergistic boost of photo-activity of ZnO for photocatalytic degradation of methylene blue by Ag decoration and Fe doping. Mater Lett. 2021;286:129250.

[20] Feng YY, Rijnaarts HHM, Yntema D, Gong ZJ, Dionysiou DD, Cao ZR, et al. Applications of anodized TiO_2 nanotube arrays on the removal of aqueous contaminants of emerging concern: a review. Water Res. 2020;186:116327.

[21] Xiang QJ, Yu JG, Wang WG, Jaroniec M. Nitrogen self-doped nanosized TiO_2 sheets with exposed [001] facets for enhanced visible-light photocatalytic activity. Chem Commun. 2011;47:6906–8.

[22] Duan JX, Huang XT, Wang EK, Ai HH. Synthesis of hollow ZnO microspheres by an integrated autoclave and pyrolysis process. Nanotechnology. 2006;17:1786–90.

[23] Dong ZH, Lai XY, Halpert JE, Yang NL, Yi LX, Zhai J, et al. Accurate control of multishelled ZnO hollow microspheres for dye-sensitized solar cells with high efficiency. Adv Mater. 2012;24:1046–9.

[24] Peng Q, Xu S, Zhuang ZB, Wang X, Li YD. A general chemical conversion method to various semiconductor hollow structures. Small. 2005;1:216–21.

[25] Zeng HC. Synthesis and self-assembly of complex hollow materials. J Mater Chem. 2011;21:7511–26.

[26] Seelig EW, Tang B, Yamilov A, Cao H, Chang RPH. Self-assembled 3D photonic crystals from ZnO colloidal spheres. Mater Chem Phys. 2003;80:257–63.

[27] Li Y, Wang YM, Liu LH, Wang DW, Zhang WL. Ag/ZnO hollow sphere composites: reusable photocatalyst for photocatalytic degradation of 17 alpha-ethinylestradiol. Env Sci Pollut R. 2014;21:5177–86.

[28] Xu M, Chen Y, Hu WY, Liu YT, Zhang QP, Yuan H, et al. Designed synthesis of microstructure and defect-controlled

Cu-doped ZnO-Ag nanoparticles: exploring high-efficiency sunlight-driven photocatalysts. J Phys D Appl Phys. 2020;53:025106.
[29] Tian CG, Zhang Q, Jiang BJ, Tian GH, Fu HG. Glucose-mediated solution-solid route for easy synthesis of Ag/ZnO particles with superior photocatalytic activity and photostability. J Alloy Compd. 2011;509:6935–41.
[30] Wu L, Dai YQ, Zeng W, Huang JT, Liao B, Pang H. Effective ion pathways and 3D conductive carbon networks in bentonite host enable stable and high-rate lithium–sulfur batteries. Nanotechnol Rev. 2021;10:20–33.
[31] Xu JQ, Xue ZG, Qin N, Cheng ZX, Xiang Q. The crystal facet-dependent gas sensing properties of ZnO nanosheets: experimental and computational study. Sens Actuat B-Chem. 2017;242:148–57.
[32] Tian SQ, Yang F, Zeng DW, Xie CS. Solution-processed gas sensors based on ZnO Nanorods array with an exposed (0001) facet for enhanced gas-sensing properties. J Phys Chem C. 2012;116:10586–91.
[33] Su X, Wang Z, Huang Y, Miao Z, Wang S, Wang J, et al. Triethanolamine interface modification of crystallized ZnO nanospheres enabling fast photocatalytic hazard-free treatment of Cr(vi) ions. Nanotechnol Rev. 2021;10(1):847–56.
[34] Kaneti YV, Zhang ZJ, Yue J, Zakaria QMD, Chen CY, Jiang XC, et al. Crystal plane-dependent gas-sensing properties of zinc oxide nanostructures: experimental and theoretical studies. Phys Chem Chem Phys. 2014;16:11471–80.
[35] Supraja P, Singh V, Vanjari SRK, Singh SG. Electrospun CNT embedded ZnO nanofiber based biosensor for electrochemical detection of Atrazine: a step closure to single molecule detection. Microsyst Nanoeng. 2020;6:3.
[36] Bhat P, Kumar SKN, Nagaraju P. Synthesis and characterization of ZnO-MWCNT nanocomposites for 1-butanol sensing application at room temperature. Phys B. 2019;570:139–47.